JOURNAL OF MATERIALS SCIENCE 33 (1998) 3047–3053

# Infiltration-processed, functionally graded aluminium titanate/zirconia–alumina composite

## Part II *Mechanical properties*

S. PRATAPA*, I. M. LOW‡
*Materials Research Group, Department of Applied Physics, Curtin University of Technology, GPO Box U1987, Perth, WA 6845, Australia*
*E-mail: rlowim@cc.curtin.edu.au*

The nature and degree of deformation-microfracture damage around Vickers indentations in a layered and graded aluminium titanate (AT)/(alumina–zirconia (AZ)) composite is studied. Samples with a homogeneous layer of AZ and a graded layer of heterogeneous AT/AZ are fabricated by an infiltration route. Depth profiling of the Vickers hardness shows that the hardness of the material is depth dependent with a relatively soft graded layer but a hard homogeneous layer. The microhardness of the graded layer is load dependent with 5.6 GPa as the asymptotic value at high loads. The evolution and accumulation of damage modes beneath Hertzian contacts are examined using "bonded-interface" sections. The stress–strain response of the material is monitored by Hertzian tests. The graded layer exhibits a distinctive "softening" in the stress–strain curve, indicating a microscale quasiplasticity which can be associated with grain debonding, grain sliding, diffuse microcracking, grain push-out and grain bridging. No contact-induced cracks are observed in the graded layer and the micro damage is widely distributed within the shear compression zone around and below the contacts. The capability of the graded material to absorb energy from the loading system and to distribute damage is somewhat akin to that of ceramics with heterogeneous microstructures. 

## 1. Introduction

The mechanical performance of ceramics is well established to be microstructure sensitive. For instance, a homogeneous and fine-grained alumina offers strength and wear and fatigue resistance but it is brittle and not damage tolerant. By judiciously adjusting the composition through addition of an appropriate amount of calcium carbonate, a microstructure of platelet calcium hexaluminate ($CaAl_{12}O_{19}$) as second phase can be produced [1]. The resultant heterogeneous microstructure showed a pronounced R-curve behaviour. A different but effective approach was adopted by other researchers [2–4] in designing flaw-tolerant alumina ceramics through uniform dispersion of aluminium titanate (AT) particles to induce intense internal residual stresses from extreme thermal expansion mismatch. When compared with single-phase alumina, alumina with uniformly distributed 20–30 vol % AT (duplex microstructure) showed much improved flaw tolerance. Further improvement in flaw tolerance was achieved through uniform incorporation of large alumina grains within a fine-grained alumina–AT matrix. (duplex–bimodal microstructure) [4]. These heterogeneous microstructures impart considerable increases in damage resistance or flaw tolerance but degrade the intrinsic strength and wear resistance. Hence, designing of ceramics may demand compromise, depending on whether one seeks toughness and flaw tolerance on the one hand, or wear and fatigue resistance on the other hand.

Recent developments in layered ceramics have provided a strategy for overcoming such compromise by laminating the ceramic structure with an outermost homogeneous layer to provide wear resistance and an underlying heterogeneous layer to provide toughness [5–7]. Unlike more traditional layered structures which promote either toughness by interlayer crack deflection or strength by incorporating macroscopic compressive residual stresses, the new approach deliberately seeks to produce strong interlayer bonding and to eliminate residual macroscopic stresses. Accordingly, any attendant counterproductive effects of weak interlayers and residual stresses, such as enhancement of delamination failures, can be avoided. Layered ceramics produced in this way by Lawn and co-workers [5–7] have shown uncommonly high damage resistance under Hertzian loading with retention of strength and wear resistance.

**Present address*: Physics Department, Faculty of Mathematics and Sciences, Institute of Technology, Sepuluh November, Surabaya, Indonesia.
‡To whom correspondence should be addressed.

0022–2461  

Here we consider a new approach, in which microstructural elements are tailored to provide graded compositions and generate different modes of strengthening and toughening. The basic idea is to produce a graded dispersion of AT within the alumina–zirconia (AZ) matrix through an infiltration process to yield a layer of homogeneous AZ for hardness and wear resistance, and a heterogeneous layer of tough graded AT/AZ for damage dispersion. This unique mechanical performance of both flaw tolerance and wear resistance has been demonstrated in the graded mullite/alumina and mullite. Zirconia-toughned alumina (ZTA) composites [8–10] where the heterogeneous layer of graded mullite/alumina or mullite/ZTA provides excellent toughness while the homogeneous alumina or ZTA layer retains strength and wear resistance. Non-oxide ceramics with excellent mechanical properties have also been synthesized by Tu and Lange [10a] using a similar infiltration process.

In this paper, Part II of the series, we present results of mechanical tests on a layered and graded AT/AZ composite processed through an infiltration method [11]. The homogeneous component is a relatively fine-grained AZ; the heterogeneous component is an AZ matrix with graded content of AT. Depth profiling of hardness and surface damage mechanisms are studied using Vickers indentations. "Bonded-interface" sections through the Hertzian contact zone are used to characterize the degree of damage accumulation beneath the graded layer. The capacity of the material to distribute damage or absorb energy from the loading system is illustrated by the non-linear indentation stress–strain curve.

## 2. Experimental procedure

### 2.1. Processing of samples

Details of processing, including infiltration, decomposition, AT formation, densification and microstructural development, were described in Part I of this series [12]. Essentially preforms were prepared by uniaxially pressing a powder mixture of AZ (10 wt % $ZrO_2$) at 37 MPa, partial sintering at 1000 °C for 2 h and infiltrating for 24 h in a solution containing 30 wt% $TiCl_4$. The infiltrated preforms were then dried at room temperature for 24 h before being heat treated at 1550 °C for 3h.

### 2.2. Elastic properties

The dimensions of bars used for the measurement of elastic properties were 3 mm × 10 mm × 50 mm. Young's modulus, $E$, of the samples was determined from the resonant frequency in the flexural mode using a resonance vibration technique [13]. The flexural modes of vibration were excited and detected using a commercial acoustic spectrometer. The half and fundamental modes were monitored by the Lissajous figure on an oscilloscope. Depth profiling of $E$ within the graded sample was done through gradual polishing of the surface with an emery paper.

### 2.3. Vickers indentations

Samples for microhardness and Vickers damage measurements were ground using SiC grinding paper and polished using diamond paste down to 1 μm. The microhardness was measured using a Zwick tester at loads in the range 0.2–300 N. At least three measurements were made for each load. In order to assess the load-dependence behaviour of microhardness in both the homogeneous and the heterogeneous layers, impressions were also performed in a load range 2–100 N. The damage mechanisms around the Vickers indentations were observed using optical and scanning electron microscopy.

### 2.4. Hertzian indentations

Information on subsurface damage during Hertzian indentations was obtained using a bonded-interface specimen configuration [14]. This test allows the nature and degree of damage accumulation beneath the indenter to be revealed. Polished surfaces of two half-specimens were glued face to face with a thin layer of adhesive under moderate clamping pressure. The top surface perpendicular to the bonded interface was polished for the indentation tests. In the Hertzian test a linear sequence of indentations was made with a WC sphere of radius, $r = 3.18$ mm, with the contacts centred across the interface trace, at peak loads up to $P = 3000$ N. The two halves of the indented specimens were then separated by dissolving the glue in acetone, cleaning, gold coating and examining using a reflection optical microscope in Nomarski interference illumination. Details of damaged surfaces at higher magnifications were examined using a scanning electron microscope (JEOL 31C).

Hertzian indentation tests were also used to determine the stress–strain curve of polished and gold-coated samples. Measurements of the contact radius, $a$, at each prescribed sphere radius, $r$, and load, $P$, were made at the impressions, to enable evaluations of indentation stress, $p_0 = P/\pi a^2$, as a function of indentation strain, $a/r$. Data were taken using a range of sphere radii, $r = 1.59$–$12.7$ mm, at loads upto $P = 3000$ N, in order to construct the stress–strain curve.

## 3. Results and discussion

### 3.1. Material characterization

Details of graded phase composition, microstructures and physical properties were presented in Part I of this series. In essence, X-ray diffraction and energy-dispersive X-ray microanalysis confirmed the graded composition within the sample; the content of AT varied from 44.5 wt % on the surface to 5.3 wt % at a depth of 1.5 mm [12]. Approximately 3.3 % open porosity was present in the graded sample compared with 2.1 % in the control.

Young's modulus, $E$, of the graded material increases with increasing polishing depth (Fig. 1), i.e., from 280 GPa for as-fired to 334 GPa at 0.3 mm depth, and then to 358 GPa at 0.5 mm depth. In comparison, the control sample has an $E$ value of 387 GPa. It is evident that the $E$ value of the graded sample approaches that of the control sample with increasing depth. The lower $E$ value in the former can be attributed to the presence of AT which decreases in content with increasing depth.

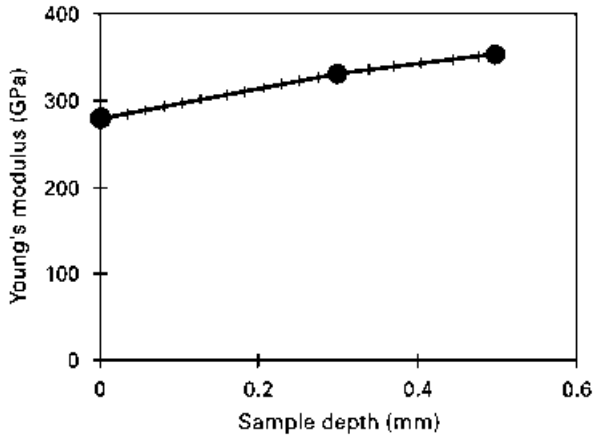


*Figure 1* Young's modulus of the graded AT/AZ composite at various depths of polishing.

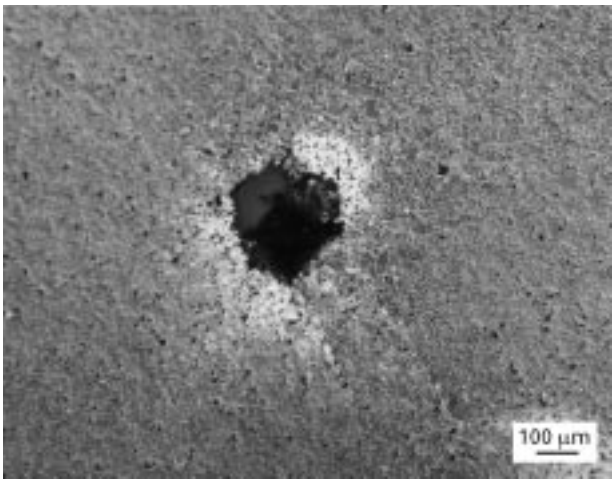


*Figure 2* Optical micrograph of the graded material showing Vickers indentation damage around the indent at 200 N load. The surface had been gold coated and viewed under Nomarski illumination.

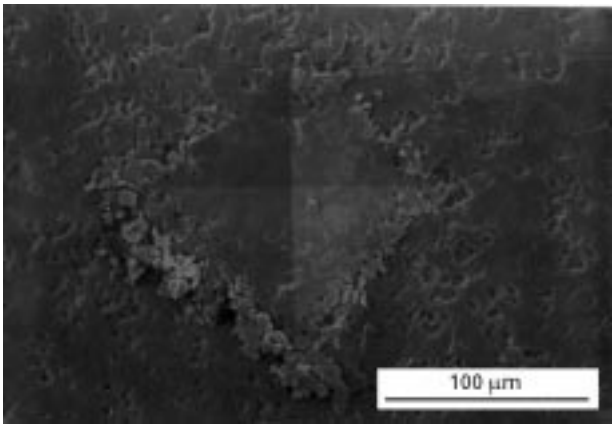


*Figure 3* Scanning electron micrograph of the graded material showing pronounced grain uplift around the indent at 100 N load.

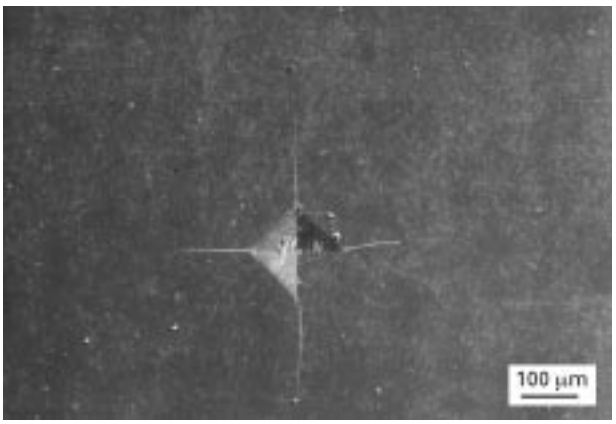


*Figure 4* Scanning electron micrograph of the control sample showing radial cracks emanating from the corners of the indent.

It is interesting to note that the graded material exhibits an excellent machinability when compared with the control sample. With the same dimensions, the time taken to cut the latter was approximately 15 times longer [11]. The fact that the graded sample is readily machinable can be correlated to its lower hardness and better "ductility" (see Sections 3.2–3.4). Similar behaviour has also been observed in mica glass–ceramics [15], SiC [16] and $Ti_3SiC_2$ ceramics [17]. As indicated from the microstructural observations, the presence of AT provides weak interphase boundaries by virtue of large thermal expansion mismatch with the AZ matrix, thus promoting the display of "quasiplastic" deformation during loading (see Section 3.3). Microscopic deformation in the system can be related to shear-driven frictional sliding at the weak interphase between AT and the matrix, resulting in interphase microfailures [15]. Such microfailures are believed to account for the "machinability" of the graded material. It follows that the poor machinability in the AZ control sample is due to the lack of such microfailures.

## 3.2. Vickers indentation and damage

Fig. 2 is an optical micrograph showing the Vickers indentation damage around the indent at 200 N load. There is a distinct upheaval in the vicinity of the indent as a result of pronounced grain uplift (Fig. 3). The presence of a profused damage zone surrounding the indent is vividly highlighted under the Nomarski illumination. However, no radial cracks are observed at 200 N. Unlike the brittle AZ control sample which exhibits cracks emanating from all four indentation corners (Fig. 4), the graded material exhibits either no cracks (up to 200 N), or short cracks in only one or two corners of the indent, at 300 N. The absence of any emanating cracks from the indent corners at 200 N was confirmed by scanning electron microscopy at high magnifications [11]. The indent tip stopped within a large grain, but no crack was generated. Grains push-out are routinely observed around the indent. Fig. 5 shows a typical observation of a grain prior to push-out and also the push-out grains (labelled G and P respectively). It is believed that, during the process of indentation, the weakly bonded grains are initially debonded, lifted up and eventually pushed out from their original positions. It appears that most of the indentation energy is used for debonding, lifting and pushing out the grains from the surface, thus rendering the material damage resistant.

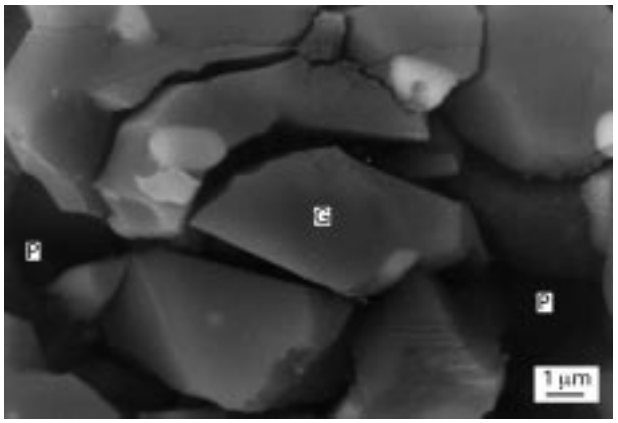


*Figure 5* High-magnification micrograph of the graded sample showing grain debonding at G and grain push-out at P.

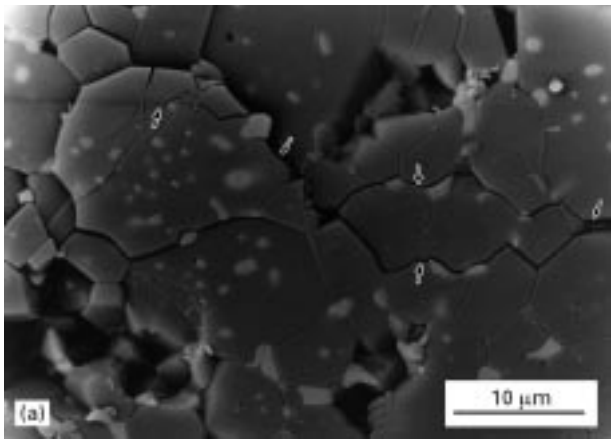


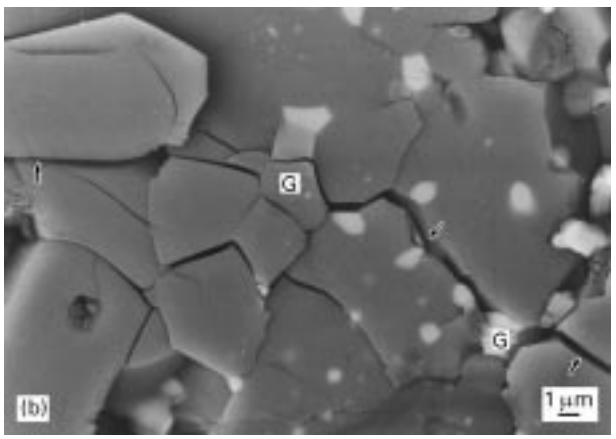


*Figure 6* Back-scattered electron micrographs of the graded sample showing (a) crack deflection and (b) grain bridging in the vicinity of an indent at 300 N. Cracks propagate from the left-hand side to the right-hand side. The arrows indicate the indentation cracks.

Fig. 6 shows the phenomena of crack deflection and grain bridging which occur in the vicinity of an indent corner on the graded material. These energy-dissipative processes have been attributed to pronounced flaw tolerance which is exhibited by the duplex or duplex–bimodal alumina–AT composites [2, 3]. The process of crack deflection is believed to arise from the presence of residual tensile stresses produced by the thermal expansion mismatch between AT and alumina.

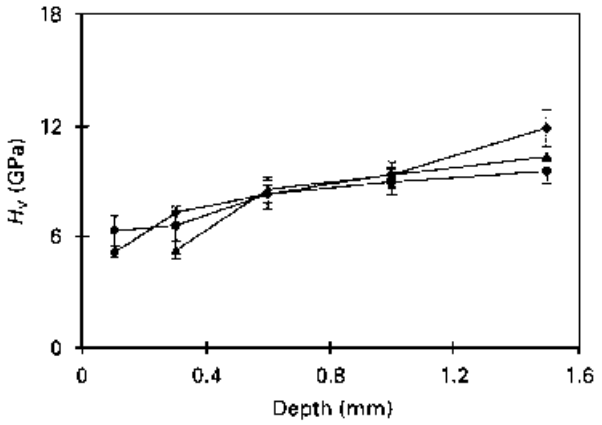


*Figure 7* Variation in Vicker's microhardness with depth of AT/AZ Functionally-graded material (FGM) for several indentation loads. (—◆—), 10 N; (—●—), 20 N; (—▲—), 100 N. Error bars indicate 2× estimated standard deviations.

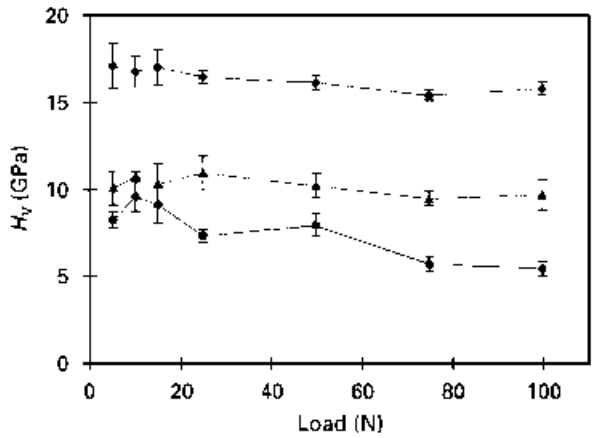


*Figure 8* Microhardness as a function of indentation load near the surface ((–●—), 0.3 mm) and at the core ((—▲—), 1.5 mm) of the AT/AZ FGM. A plot for the control specimen is also presented (—◆—). Error bars indicate 2× estimated standard deviations.

It should be pointed out that the display of profused grain uplift and microdamage around the indent (see Figs 2 and 3) is unusual for ceramic materials. When an indentation is applied, ceramics usually exhibit a "sink in impression" which is caused by the densification below the tip of indent [18]. This is usually accompanied by the formation of radial cracks at the four corner tips of the indents, indicating the brittleness of the material. By contrast, metals usually exhibit a "rising material" or surface uplift above the unindented surface level as a result of shear or plastic deformation. It follows that the graded material exhibits indentation damage patterns which are indicative of pseudoplastic deformation during loading. The presence of AT "softens" the AZ matrix, thus rendering it effective in energy absorption and crack attenuation.

As would be expected, the microhardness, $H_V$, of the graded material increases with depth (Fig. 7), since the concentration of relatively soft AT decreases with depth [12]. The microhardness of the graded layer as a function of applied load is shown in Fig. 8. At higher loads, the hardness approaches asymptotically a value of approximately 5.6 GPa. At lower loads, the hardness values increase with decreasing load levels and

reach a maximum value of 9.5 GPa at 2 N. This load-dependent microhardness behaviour is very pronounced near the surface region and becomes less apparent as the core region is approached. A similar phenomenon has been widely observed in metal-like ceramics such as $Ti_3SiC_2$ [19–21], which can be correlated to the "quasiductility" of the material.

Further evidence in support of the surface "ductility" of the graded material is its low $H_V/E$ ratio. For brittle materials, it has been found that the microhardness does not depend on load and the $H_V/E$ ratio ranges from 0.04 to 0.1 whereas, for hard metals, the microhardness is load-dependent and $H_V/E$ ranges from 0.001 to 0.03 [22]. The load dependence of microhardness in the graded material is evident from Fig. 8. With an average hardness of 5.6 GPa and Young's modulus of 280 GPa, graded material has a $H_V/E$ value of 0.02, which is notably comparable with that of the hard metals. This result, once again, indicates that the near-surface region of the graded material exhibits a high degree of "quasiductility" which diminishes with increasing depth.

### 3.3. Hertzian indentation and damage

The stress–strain curves obtained from spherical indentations on both graded and control samples are illustrated in Fig. 9. The broken line through the origin is the elastic curve computed from Hertzian theory [23]:

$$P_0 = \left(\frac{3E}{4\pi k}\frac{a}{r}\right) \quad (1)$$

where $E$ is Young's modulus of the material and $k$ is taken as 0.88 [24]. The upper broken line is an indentation hardness obtained from Vickers tests. The solid

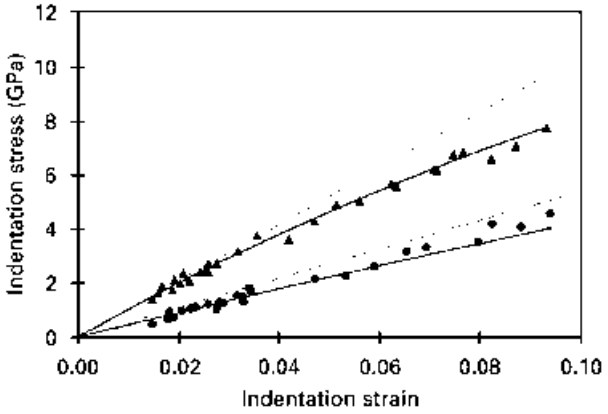


*Figure 9* Indentation stress–strain curves for both graded (●) and control (▲) samples. (——), empirical fits.

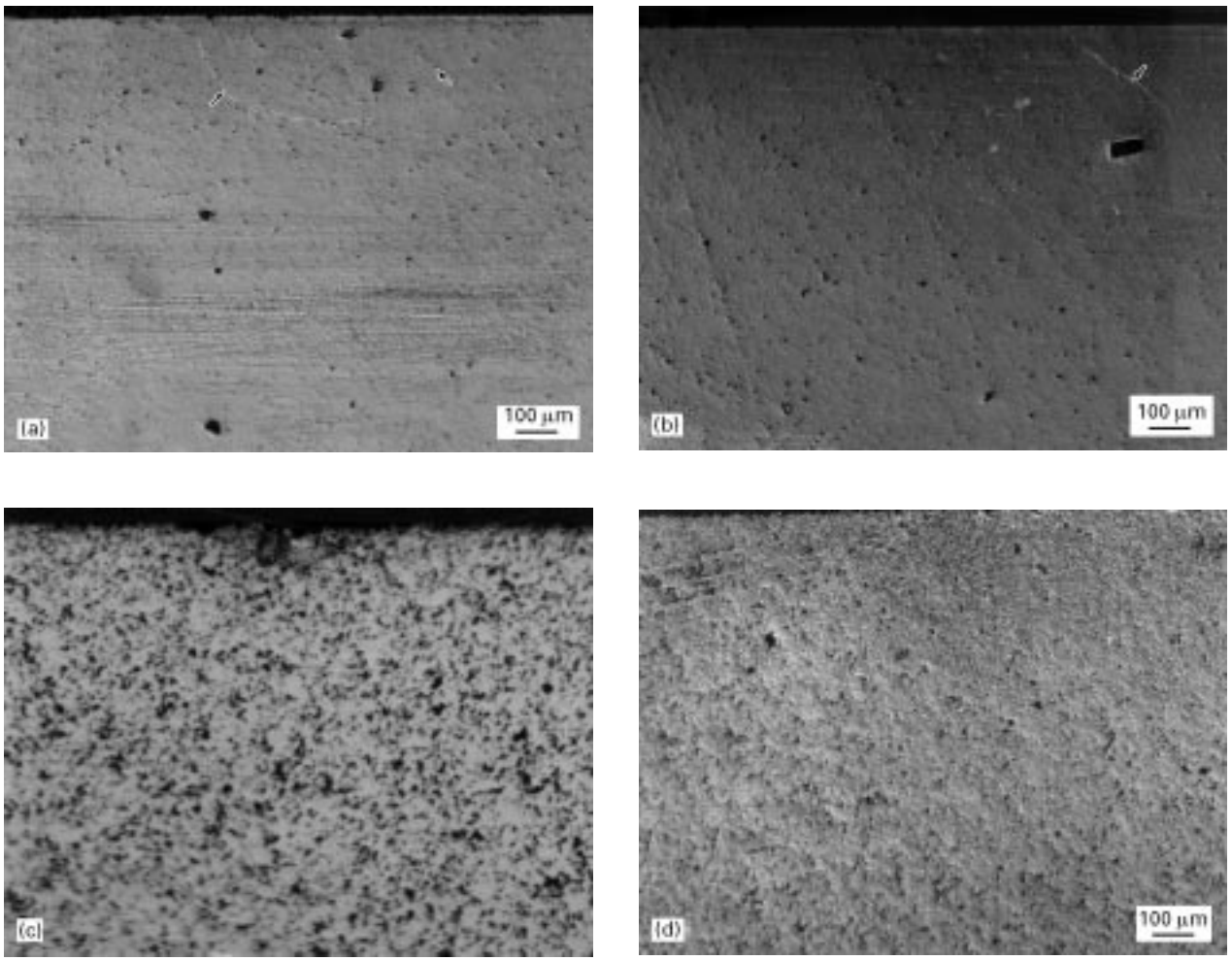


*Figure 10* Optical micrographs in Nomarski illumination showing (a), (c), (e), (g) half-surface and (b), (d), (f), (h) section views of Hertzian damage in both graded and control samples. Indentations made with WC ball of radius $r = 3.18$ mm at increasing contact loads: (a), (b) control sample at $P = 2$ kN; (c), (d) graded sample at $P = 0.3$ kN; (e), (f) graded sample at $P = 0.85$ kN, (g), (h) graded sample at $P = 2.0$ kN.

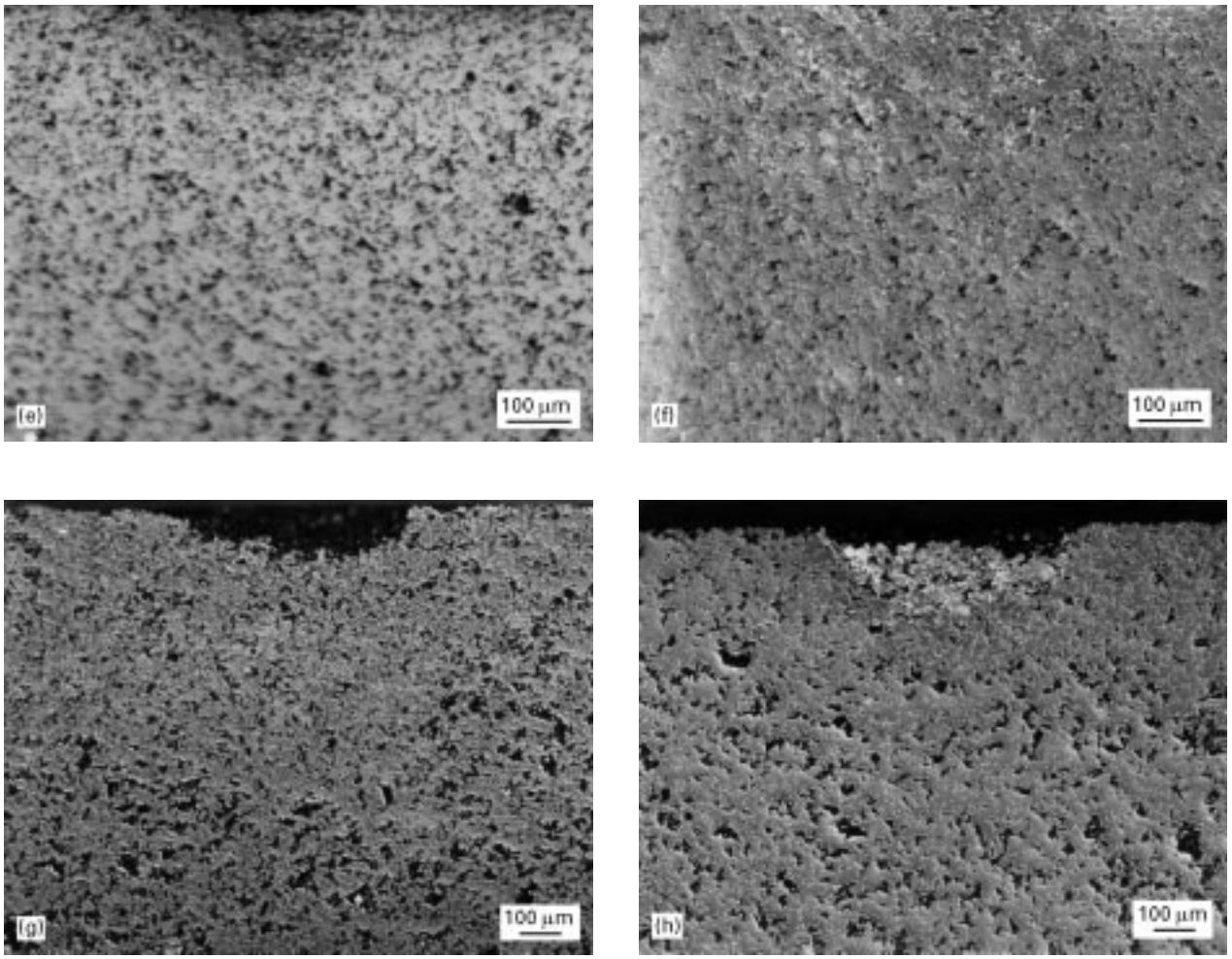


*Figure 10* (continued)

curves are empirical fits to the data. The data deviate below the Hertzian line at stresses above $P_0 \approx 2$ GPa for the control and $P_0 \approx 0.4$ GPa for the graded sample, marking the onset of "yield". This result serves to verify the "quasiplastic" nature of the graded material, a phenomenon which has also been observed in other ceramics with a heterogeneous microstructure [5–7].

Optical microscopy confirms that the "yielding" behaviour during Hertzian loading arises from the onset of indentation damage in the graded material. The nature of this damage can be discerned from the micrograph sequences in Fig. 10, obtained using the bonded-interface section technique previously described. The micrographs show both half-surface (upper) and section views (lower) of indentations. The results clearly show the evolution of subsurface damage development as one progresses up the stress–strain curve in Fig. 9 which corresponds to increasing indentation pressure. The initiation of the shear-driven subsurface damage zone, and subsequent expansion of this zone, are immediately apparent from the grain deformations or displacements revealed by the Nomarski contrast. At $P_0 \approx 0.5$ GPa, i.e., just above the elastic limit, only a few grains have deformed through shear-driven debonding, sliding, diffuse microcracking and push-out. The debonded and push-out grains are readily removed during ultrasonic cleaning of the bonded-interface sections in acetone. This feature of grain removal from the surface is vividly portrayed in Fig. 10. With increasing pressure, the number of deformed grain increases, and the damage zone expands further below the surface. At $P_0 \approx 2.0$ GPa, the damage is more profuse and begins to take on the appearance of the well-developed near-hemispherical deformation zone expected from continuum plasticity models [25]. The complete absence of any ring cracks or cone cracks on the surfaces, even at the maximum pressure, suggests that the graded material is damage tolerant. Cone fracture is inhibited by the ability of the material to contain the extent of microdamage to a small area around the indent via multiple energy-absorbing mechanisms which include diffuse microcracking, grain debonding and sliding, crack deflection, grain push-out and grain bridging. In contrast, a ring crack on the surface of the control sample has initiated and attempted to run around the contact circle. The classical cone crack has also formed in the subsurface region, highlighting the brittleness of this material.

## 4. Conclusions

An infiltration route was used to fabricate samples with a homogeneous AZ layer and a graded heterogeneous AT/AZ layer. The damage modes surrounding Vickers and Hertzian contacts in the material have been studied. The resultant material is damage

tolerant and exhibits graded mechanical properties. The graded surface layer has a lower Young's modulus and hardness than the non-graded core. These graded changes in properties are related to the presence of AT, which gradually reduces in amount from the surface to the core.

When compared with the homogeneous AZ, the graded AT/AZ material demonstrates better mechanical performances which include (a) enhanced quasi-plasticity and flaw tolerance through its capacity to distribute microdamage and (b) improved "machinability" by virtue of profuse shear-induced weak interfaces. This material is expected to exhibit improved thermal shock resistance [26] in view of its lower thermal expansion coefficient and better ability in crack attenuation.

## Acknowledgements

S. Pratapa is very grateful to the Australian Agency for International Development for providing a scholarship. I. Low is grateful to the Australian Research Council and the Australian Institute of Nuclear Science and Engineering (AINSE) for financial support (AINSE Grant 96/142), and to Professor K. Niihara of Osaka University, Japan, and Dr B. Lawn of the National Institute of Standard and Technology, Maryland, USA, for providing facilities to perform measurements of Young's modulus and Hertzian contact damage respectively. We thank Professor B. O'Connor and Ms E. Miller for proof reading and assistance with scanning electron microscopy, respectively.

## References

1. L. AN, H. M. CHAN and K. K. SONI, *J. Amer. Ceram. Soc.* **79** (1996) 3142.
2. L. M. BRAUN, S. J. BENNISON and B. R.LAWN, *ibid.* **75** (1992) 3049.
3. J. L. RUNYAN and S. J. BENNISON, *J. Eur. Ceram. Soc.* **7** (1991) 93.
4. N. P. PADTURE, S. J. BENNISON and H. M. CHAN, *J. Amer. Ceram. Soc.* **76** (1993) 2312.
5. L. AN, H. M. CHAN, N. P. PADTURE and B. R. LAWN, *J. Mater. Res.* **11** (1996) 204.
6. N. P. PADTURE, D. C. PENDER, S. WUTTIPHAN and B. R. LAWN, *J. Amer. Ceram. Soc.* **78** (1995) 3160.
7. H. LIU, B. R. LAWN and S. M. HSU, *ibid.* **79** (1996) 1009.
8. B. R. MARPLE and D. J. GREEN, *ibid.* **74** (1991) 2453.
9. I. M. LOW, R. SKALA and D. S. PERERA, *J. Mater. Sci. Lett.* **13** (1994) 1334.
10. S. PRATAPA and I. M. LOW, *ibid.* **15** (1996) 800.

10a. W. C. TU and F. F. LANGE, *J. Amer. Ceram. Soc.* **78** (1995) 3283.

11. S. PRATAPA, M.Sc Thesis, Curtin University of Technology, Perth (1997).
12. S. PRATAPA, I. M. LOW and B. H. O'CONNOR, *J. Mater. Sci.* (1998) submitted.
13. E. SCHREIBER, D. L. ANDERSON and N. SOGA, "Elastic constants and their measurements" (McGraw-Hill, New York, 1973).
14. F. GUIBERTEAU, N. P. PADTURE, H. CAI and B. R. LAWN, *Phil. Mag. A* **68** (1993) 1003.
15. C. K. CHYUNG, G. H. BEALL and D. G. GROSSMAN, in "Electron microscopy and structure of materials", edited by G. Thomas, R.M. Fulrath and R.M. Fisher. (University of California Press, Berkeley, CA, 1972) pp 1167–94
16. N. P. PADTURE, C. J. EVANS, H. K. XU and B. R. LAWN, *J. Amer. Ceram. Soc.* **78** (1995) 215.
17. M. W. BARSOUM and T. EL-RAGHY, *ibid.* **79** (1996) 1953.
18. K. ZENG, E. SOEDERLUND, A. E. GIANNAKOPOULOS and D. J. ROWCLIFFE, *Acta Mater.* **44** (1996) 1127.
19. T. GOTO and T. HIRAI *Mater. Res. Bull.* **22** (1987) 2295.
20. R. PAMPUCH, J. LIS, J. PIEKARCZYK and L. STOBIERSKI, *J. Mater. Synth. Processing* **1** (1993) 93.
21. T. EL-RAGHY, A. ZAVALIANGOS, M. BARSOUM and S. R. KALIDINDI, *J. Amer. Ceram. Soc.* **80** (1997) 513.
22. I. J. McCOLM, "Ceramic hardness" (Plenum, New York, 1990).
23. M.V. SWAIN and B. R. LAWN, *Phys. Status Solidi* **35** (1969) 909.
24. K. L. JOHNSON, "Contact mechanics" (Cambridge University Press, London, 1985).
25. D. TABOR, "Hardness of metals" (Clarendon, Oxford, 1951).
26. C. STONE, Department of Applied Physics, Curtin University of Technology, Perth, Australia, Physics Project 391 Interim Report.

*Received 12 August 1997*
*and accepted 18 March 1998*